HAL
open science

Fast electrochemical storage process in sputtered Nb2O5 porous thin films

Cassandra Arico, Saliha Ouendi, Pierre-Louis Taberna, Pascal Roussel, Patrice Simon, Christophe Lethien

To cite this version:

Cassandra Arico, Saliha Ouendi, Pierre-Louis Taberna, Pascal Roussel, Patrice Simon, et al.. Fast electrochemical storage process in sputtered Nb2O5 porous thin films. ACS Nano, 2019, 13 (5), pp.5826-5832. 10.1021/acsnano.9b01457 . hal-02263481

HAL Id: hal-02263481

https://hal.science/hal-02263481v1

Submitted on 12 Nov 2019

HAL is a multi-disciplinary open access archive for the deposit and dissemination of scientific research documents, whether they are published or not. The documents may come from teaching and research institutions in France or abroad, or from public or private research centers.

L'archive ouverte pluridisciplinaire **HAL**, est destinée au dépôt et à la diffusion de documents scientifiques de niveau recherche, publiés ou non, émanant des établissements d'enseignement et de recherche français ou étrangers, des laboratoires publics ou privés.

Open Archive Toulouse Archive Ouverte (OATAO)

OATAO is an open access repository that collects the work of Toulouse researchers and makes it freely available over the web where possible

This is an author's version published in: http://oatao.univ-toulouse.fr/24650

Official URL: https://doi.org/10.1021/acsnano.9b01457

To cite this version:

Arico, Cassandra and Ouendi, Saliha and Taberna, Pierre-Louis and Roussel, Pascal and Simon, Patrice and Lethien, Christophe *Fast Electrochemical Storage Process in Sputtered Nb2O5 Porous Thin Films.* (2019) ACS Nano, 13 (5). 5826-5832. ISSN 1936-0851

Any correspondence concerning this service should be sent to the repository administrator: tech-oatao@listes-diff.inp-toulouse.fr

Fast Electrochemical Storage Process in Sputtered Nb_2O_5 Porous Thin Films

Cassandra Arico,[†,‡,§] Saliha Ouendi,[†,§] Pierre-Louis Taberna,[‡,§] Pascal Roussel,[∥] Patrice Simon,[*,‡,§] and Christophe Lethien[*,†,§]

[†]Institut d'Electronique, de Microélectronique et de Nanotechnologie, Université de Lille, CNRS, Centrale Lille, ISEN, Université de Valenciennes, UMR 8520-IEMN, F-59000 Lille, France

[‡]Centre Interuniversitaire de Recherche et d'Ingénierie des Matériaux (CIRIMAT), CNRS UMR 5085, Université Paul Sabatier, 118 Route de Narbonne, 31062 Toulouse, France

[§]Réseau sur le Stockage Electrochimique de l'Energie (RS2E), CNRS FR 3459, 33 Rue Saint Leu, 80039 Amiens Cedex, France

[∥]Unité de Catalyse et de Chimie du Solide (UCCS), Université de Lille, CNRS, Centrale Lille, ENSCL, Université d'Artois, UMR 8181−UCCS, F-59000 Lille, France

Supporting Information

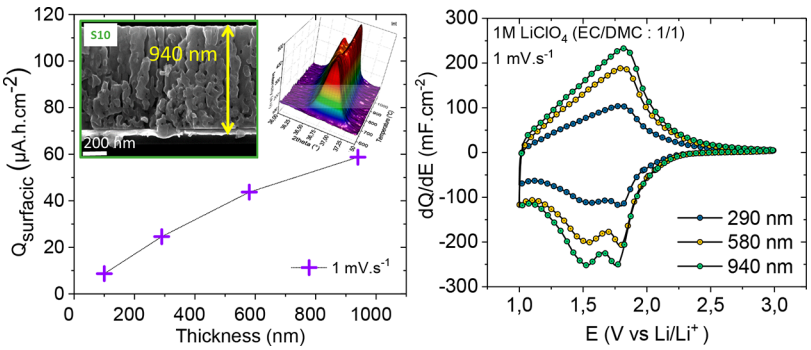

ABSTRACT: **The formation of a thin film electrode exhibiting high capacity and high rate capabilities is challenging in the field of miniaturized electrochemical energy storage. Here, we present an elegant strategy to tune the morphology and the properties of sputtered porous Nb_2O_5 thin films deposited on Si-based substrates *via* the magnetron sputtering deposition technique. Kinetic analysis of the redox reactions is studied to qualify the charge storage process, where we observe a non-diffusion-controlled mechanism within the porous niobium pentoxide thin film. To improve the surface capacity of the Nb_2O_5 porous electrode, the thickness is progressively increased up to 0.94 μm, providing a surface capacity close to 60 μAh·cm^{-2} at 1 mV·s^{-1}. The fabrication of high energy density miniaturized power sources based on the optimized T-Nb_2O_5 films could be achieved for Internet of Things applications requiring high rate capability.**

KEYWORDS: *Nb_2O_5, sputtering, thin film, lithium intercalation, fast kinetics*

Powering wireless nodes is one of the major challenges within society for the future Internet of Things (IoT), where embedded electronics devices and sensors are connected together to collect and exchange data.[1] Indeed, continuous development and further miniaturization of electronic devices such as smartphones, GPS, and tablets greatly stimulate research on the fabrication of small and compact electrochemical energy storage (EES) sources. These small footprint area EES sources have to be efficient in terms of energy, power density, cyclability, and lifespan and should be directly integrated on chips to allow the development of autonomous, sustainable, and connected IoT devices.[2,3] To significantly improve the energy density of miniaturized electrochemical capacitors (micro-supercapacitor, MSC) while keeping the power capability of such small devices high,[4] a specific class of microdevices with high energy and power densities able to charge and discharge at high cycling rates has to be developed. To reach this goal, the micro-supercapacitor topology moves from a symmetric configuration (carbon/carbon, RuO_2/RuO_2, *etc.*)—taking into account capacitive or pseudocapacitive electrodes—to a hybrid one. Combining the advantage of a capacitive electrode with that of a high-power battery electrode (microbatteries, MB) in an organic electrolyte is an attractive solution to fulfill the requirements. In fact, the energy density of electrochemical capacitors changes with the

DOI: 10.1021/acsnano.9b01457

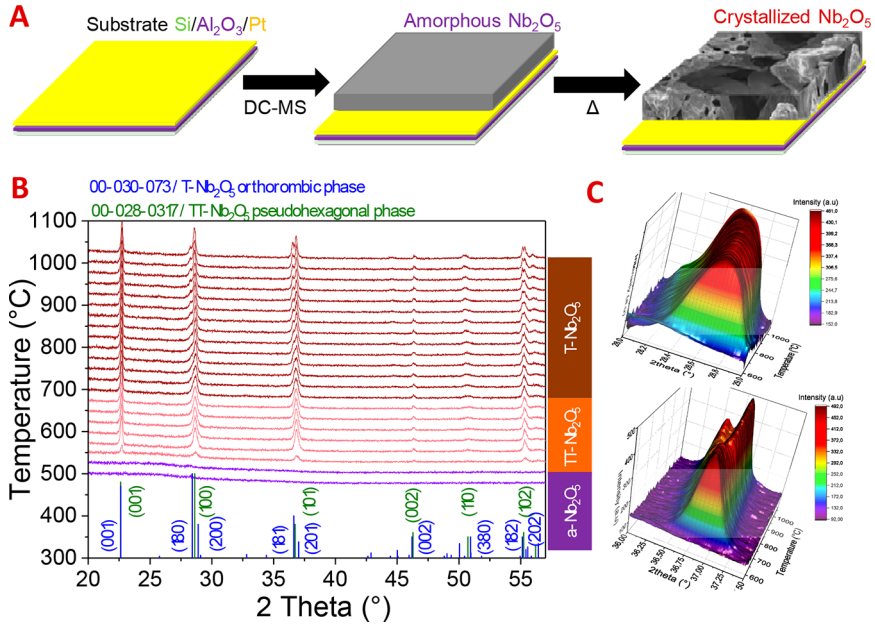

Figure 1. (A) Overview of the electrode design for hybrid microdevices: an amorphous layer is deposited by dc-MS and annealed to form the desired Nb_2O_5 polymorphs (TT-Nb_2O_5 or T-Nb_2O_5). (B) Evolution of the Nb_2O_5 crystalline phase as a function of the annealing temperature in high-resolution parallel beam configuration. High-temperature XRD patterns of Nb_2O_5 film deposited on a Si wafer as a function of the annealing temperature, from 500 up to 1050 °C under an air atmosphere. (C) Focus on the diffraction peaks at 2θ = 28.5° and 36.7° corresponding to the (180), (200) and (181) (201) planes of the orthorhombic phase, respectively, and (100), (101) of the hexagonal one.

voltage squared; as a result, an increase from 1 V (typical cell voltage value when operating in aqueous electrolyte) to 3 V leads to a 9-fold increase in the energy density. This is the reason that one important challenge for supercapacitors and micro-supercapacitors is to use high (pseudo)capacitive materials operating in a large potential window. However, transferring the hybridation concept,[5] which combines a faradic electrode with a capacitive-like electrode, from the macroscale down to the microscale is challenging. Such a combination allows improving the energy density thanks to the faradic contribution of the battery-type electrode and higher cell voltage. Recently, numerous Li-ion battery (LIB) materials for high-power applications have been investigated where nanosized, highly conductive, and porous-shaped particles are the three key parameters allowing producing high cycling rate and high energy density electrodes. As a matter of fact, materials achieving fast lithium ion intercalation *via* non-diffusion-controlled reaction kinetics have been prepared, such as MoO_3,[6,7] TiO_2,[8−12] MoO_2,[13] $LiMnO_2$,[14] and Nb_2O_5.[15−17]

Charge storage in Nb_2O_5 occurs through the intercalation of lithium ions with concomitant reduction of Nb^{5+} to Nb^{4+} expressed as

$$Nb_2O_5 + xLi^+ + xe^- \rightarrow Li_xNb_2O_5 \quad (1)$$

where $x = 2$ corresponds to the maximum theoretical capacity[18] of 200 mAh·g^{-1}. To improve the energy density of the carbon-based MSC, the use of Nb_2O_5 as electrode active materials is promising, as already reported for a classical electrochemical capacitor (EC).[19]

Nb_2O_5 is an insulating material ($\sigma_{elec} \approx 3 \times 10^{-6}$ S·cm^{-1})[20,21] and exhibits 16 polymorphs, which can be obtained mainly through thermal treatments.[15] The formation of each Nb_2O_5 polymorph depends on the initial precursors, synthesis methods, and heat treatment conditions. The crystalline pseudohexagonal TT-Nb_2O_5 and orthorhombic T-Nb_2O_5 phases exhibit Li^+ intercalation where a continuous change of potential with state of charge indicates that the lithium intercalation occurs with a single-phase material since their crystalline structure offers suitable transport pathways. B. Dunn *et al.*[16,17,22] have shown that the orthorhombic form of Nb_2O_5 (T-Nb_2O_5) could deliver high capacitance at high rate (up to 1000C), confirming the fast lithium ion intercalation/deintercalation processes in such a bulk porous and nanostructured material.[16]

Integrating Nb_2O_5 material into small IoT devices requires the miniaturization of the EES source; in that aim, the use of thin film electrodes synthesized by vapor deposition techniques offers attractive opportunities. The fabrication process on silicon chips has to be compatible with the facilities used in the microelectronic industry. Among existing thin film deposition technologies to produce binder-free electrodes,[24] magnetron sputtering is a powerful tool where the film structure and properties can be tuned according to the deposition parameters (sputtering power, gas pressure, deposition temperature, deposition time).

The present study aims at depositing porous Nb_2O_5 thin films by a dc sputtering technique from a metallic niobium target under an Ar/O_2 atmosphere. To reach this goal, the pressure is tuned to study the evolution of the film morphology from compact to porous shape. The as-deposited film is then annealed to transform the amorphous Nb_2O_5 (a-Nb_2O_5) thin films into porous crystallized TT-Nb_2O_5 or T-Nb_2O_5 films exhibiting high capacity at high cycling rate. Once the optimization of the electrochemical properties is reached, the electrode performance has to be maximized: hence, we study the increasing of the film thickness while keeping porous the film morphology to promote the fast lithium interaction process in the crystallized Nb_2O_5 layers.

RESULTS AND DISCUSSION

Optimization of the Annealing Temperature. As mentioned previously, the purpose of this study is thus to prepare sputtered and crystallized Nb_2O_5 porous thin films able to favor the fast Li-ion transport along specific crystallographic pathways (Figure 1A). In this regard, *in situ* high-temperature X-ray diffraction (HT-XRD) analysis is performed on the as-deposited sample to determine the crystallization temperatures of the Nb_2O_5 polymorphs. Nb_2O_5 (0.1 μm thick) thin films deposited at 10^{-2} mbar on a silicon wafer resulted in the formation of amorphous Nb_2O_5 (a-Nb_2O_5). XRD patterns are recorded during an annealing process every 25 °C from 50 to 1100 °C in order to determine the annealing temperatures required to reach the formation of the different Nb_2O_5 polymorphs. Figure 1B shows clearly a three-step process. From room temperature (RT) to 550 °C, the niobium pentoxide thin film is amorphous (a-Nb_2O_5). Starting from 575 °C, the pseudohexagonal structure TT-Nb_2O_5 is identified (JCPDS 00-028-0317). A splitting of the diffraction peaks (Figure 1C) at 2θ = 28° and 36.5° is observed when the annealing temperature is higher than 650 °C, resulting from the formation of the orthorhombic polymorph T-Nb_2O_5 (JCPDS 00-030-0873). From 650 to 700 °C, a mix between the TT-Nb_2O_5 and the T-Nb_2O_5 phases is observed, and at temperature higher that 700 °C the pure T-Nb_2O_5 expected phase is obtained.

Based on these structural conclusions, sputtered Nb_2O_5 thin films deposited on an Al_2O_3/Pt current collector are *ex situ* annealed during 2 h under an air atmosphere at 700 °C to obtain the expected orthorhombic phase.[23] Scanning electron microscopy (SEM) cross section imaging, *ex situ* X-ray diffraction analyses, and cyclic voltammetry between 1 and 3 V *vs* Li/Li^+ are shown in Figure SI1. The film morphology is found to be highly dense and homogeneous. From the corresponding XRD pattern, a preferential orientation is observed since only the diffraction peak of the (181) plane is visible (Figure SI1-B). From an electrochemical point of view, the observed signature is the expected one. A drastic loss of current during the first cycle and a delamination of the thin film from the substrate is observed (Figure SI1-C). Such delamination is classically observed when the mechanical stress in the film is high and/or when the thin film crystalline network does not offer suitable transport pathways required for Li^+ intercalation. In these T-Nb_2O_5 films (100 nm thick), the stress is known to be high regarding both the film density (4 g·cm^{-3}) and the absence of columnar morphology with intra- and intercolumnar porosities.[24−26] Moreover, as already pointed out, our thin film exhibits a strong preferential orientation along only one direction plane without the [001] crystallographic direction, the most energetically favorable pathways for facile Li.[27] To avoid these problems, the Nb_2O_5 microstructure has to be porous, stress free, without any cracks or failures, and polycrystalline. Such morphology is similar to the T-Nb_2O_5 nanoparticles synthesized by B. Dunn *et al.*[22] and also enhances the material/electrolyte interface area.

To produce such a porous T-Nb_2O_5 film by a sputtering technique, a tuning of both the sputtering deposition conditions within the chamber and of the thermal treatment is achieved to fulfill the electrochemical performance requirements.

Tuning of the Film Morphology with the Deposition Pressure. Table 1 summarizes the deposition parameters of as-deposited Nb_2O_5 obtained at different pressures, deposition times, and annealing temperatures (samples 1 to 10). Figure 2A shows the SEM cross section of sputtered Nb_2O_5 thin films obtained at different pressure conditions and annealed at T = 700 °C under N_2 (samples S1−S4). The melting point of the Nb_2O_5 compound is T_a = 1793.15 K. For depositions at room temperature, the $\frac{T}{T_m}$-ratio is lower than 0.2 and the film morphology is found to be in zone T from the Thornton structure zone model (SZM). Indeed, at low pressure (samples S1 and S2) thin films exhibit dense granular-like structure, and the surface roughness is very low (∼2 nm). The film densification at low pressure is a consequence of the peening effect and can induce mechanical stress of the thin film. When the pressure is increased (S3 and S4), the morphology moves to a porous granular-like structure with a surface roughness that is still low (∼4.5 nm).

Table 1. Deposition and Annealing Conditions of the Samples under Test

pressure (mbar)	thickness (nm)	time (min)	annealing (°C)	sample name
7.5×10^{-3}	100	20	700	S1
1×10^{-2}	100	24	700	S2
2.5×10^{-2}	100	30	700	S3
5×10^{-2}	100	30	700	S4
2.5×10^{-2}	100	30	600	S5
2.5×10^{-2}	100	30	650	S6
2.5×10^{-2}	100	30	750	S7
2.5×10^{-2}	290	90	650	S8
2.5×10^{-2}	580	180	650	S10
2.5×10^{-2}	940	270	650	S11

To obtain a stable Nb_2O_5 microstructure without cracks and failures, the stress induced by the Nb_2O_5 films grown on the silicon wafer has to be investigated. For that purpose, the curvature radius before and after the sputtering deposition has been measured and the film stress evaluated using the Stoney formula (Figure 2B). The mechanical stress is minimized at 0.75 $\times 10^{-2}$ and 2.5×10^{-2} mbar deposition pressure. Nevertheless, to deposit Nb_2O_5 thin films without cracks and failures, the higher pressure (2.5×10^{-2} mbar) offers the best compromise between the roughness and the mechanical stress.

In addition, the kinetics of the lithium ion intercalation process as a function of pressure for T = 700 °C is examined. Figure 2C shows the cyclic voltammetries (CVs) of the four samples (S1 to S4) at 1 mV·s^{-1} in 1 M $LiClO_4$ in ethyl carbonate (EC)/dimethyl carbonate (DMC) (1:1) between 1.0 and 3.0 V *vs* Li/Li^+. The four cyclovoltamograms are different due to the type of Nb_2O_5 polymorphs obtained according to the deposition pressure. As a matter of fact, if the pressure is higher than 2.5×10^{-2} mbar, the film exhibits a T-Nb_2O_5 orthorhombic structure, as depicted in the diffractograms reported in Figure SI2. Two strong (180) and (200) diffraction peaks occurring at 28.5° are observed, suggesting fast lithium ion transport in such crystallographic pathways. When the pressure is lower than 2.5×10^{-2} mbar, the TT-Nb_2O_5 polymorph is clearly highlighted: only one peak is observed at 28.5°. Therefore, the CVs of samples S3 and S4 are different from the CVs of samples S1 and S2 regarding the number of reduction peaks. A similar observation was reported by B. Dunn *et al.*[16] in 2012. The Nb_2O_5 film deposited at 2.5×10^{-2} mbar exhibits higher capacitance and rate capability, demonstrated by the reversible electrochemical signature and the largest current response. The porous microstructure of the sputtered Nb_2O_5 films at high pressure is assumed to be responsible for the fast intercalation process of the lithium ion within the bulk material.

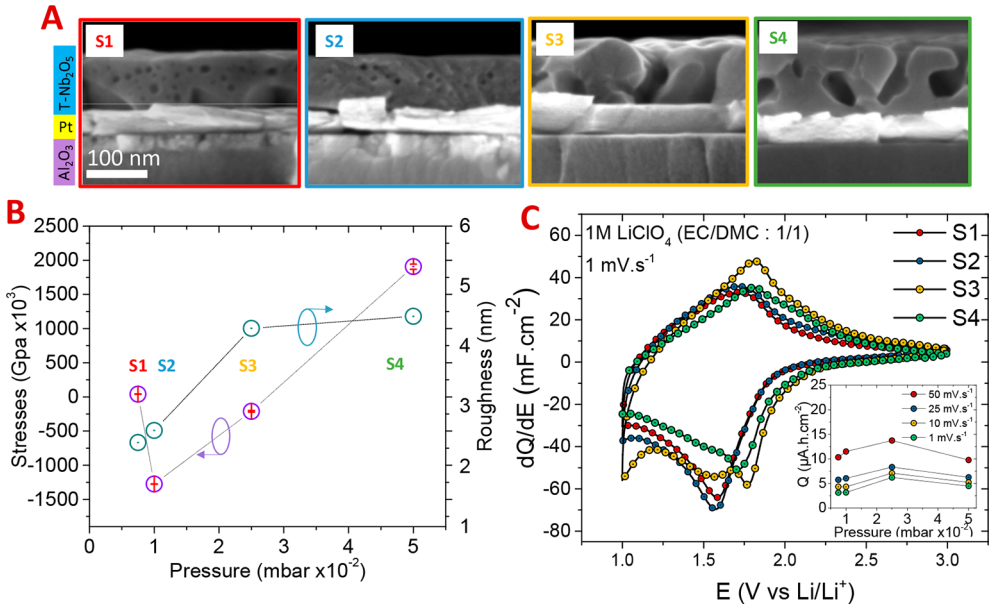

Figure 2. Study of 100 nm thick Nb_2O_5 thin films deposited at different pressures (0.75, 1, 2.5, and 5 × 10^{-2} mbar). All the layers are annealed at 700 °C under N_2 during 5 min. (A) SEM cross section analyses as a function of the deposition pressure. (B) Evolution of the intrinsic stress and the roughness regarding the deposited pressures. (C) Cyclic voltamperometry at 1 mV·s^{-1} between 1 and 3 V *vs* Li/Li^+ of the four studied Nb_2O_5 layers. The inset reports the surface capacity as a function of the pressure at different sweep rates. From this study, a deposition pressure at 2.5 × 10^{-2} mbar provides the optimal electrochemical performance.

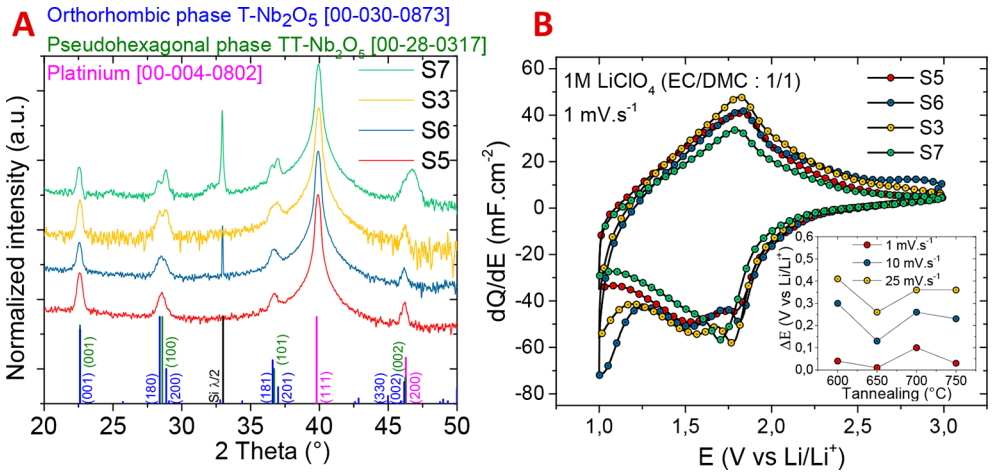

Figure 3. (A) X-ray diffraction analysis of Nb_2O_5/Pt/Al_2O_3/Si samples regarding the annealing temperature (P = 2.5 × 10^{-2} mbar kept constant), from 600 up to 750 °C (the diffractograms are normalized to the (111) peak of Pt at ~40°). All the samples are annealed under N_2 during 5 min. (B) Cyclic voltammetry at 10 mV·s^{-1} between 1 and 3 V *vs* Li/Li^+ of the four samples, demonstrating the dependent redox activity with the crystalline polymorphic structure. The inset reports the potential difference between the oxidation and reduction peaks as a function of the annealing temperature at different sweep rates. From this study, an annealing temperature of 650 °C provides the optimal electrochemical performance (more reversible CV and lower ΔE).

Then, the influence of annealing treatment was studied. For that purpose, Nb_2O_5 films deposited at 2.5 × 10^{-2} mbar have been annealed during 5 min under a N_2 atmosphere at 600, 650, 700, and 750 °C (rapid thermal annealing process).

The XRD of the S3, S5, S6, and S7 samples is shown in Figure 3A and confirms that all the thin films are polycrystalline (no preferential orientation is observed whatever the annealing temperature is). Here also, the formation of the TT-Nb_2O_5 polymorph is observed between 550 and 650 °C, a mix between the TT-Nb_2O_5 and T-Nb_2O_5 phases is achieved at 650 °C, while the synthesis of the T-Nb_2O_5 occurs beyond 650 °C.

Figure 3B shows the CV analysis of the TT-Nb_2O_5, T-Nb_2O_5, and mixed phase films at 1 mV·s^{-1} in 1 M $LiClO_4$–EC/DMC (1:1). Based on the potential difference (inset) between the oxidation/reduction peaks at 1.7 V *vs* Li/Li^+, the fast lithium intercalation/deintercalation process is more reversible in the TT-Nb_2O_5/T-Nb_2O_5 mixed phase at 650 °C compared to the others.

Based on these optimizations, the deposition pressure and annealing temperature are fixed at 2.5 × 10^{-2} mbar and at 650 °C under N_2 during 5 min, respectively: in that case, a mixed phase is obtained.

Figure 4A shows cyclic voltammetries for sweep rates between 1 and 100 mV·s^{-1}. For sample S8 (300 nm thick) deposited at 2.5 × 10^{-2} mbar two broad cathodic peaks at about 1.5 and 1.8 V *vs* Li/Li^+, corresponding to Li-ion intercalation into Nb_2O_5, are

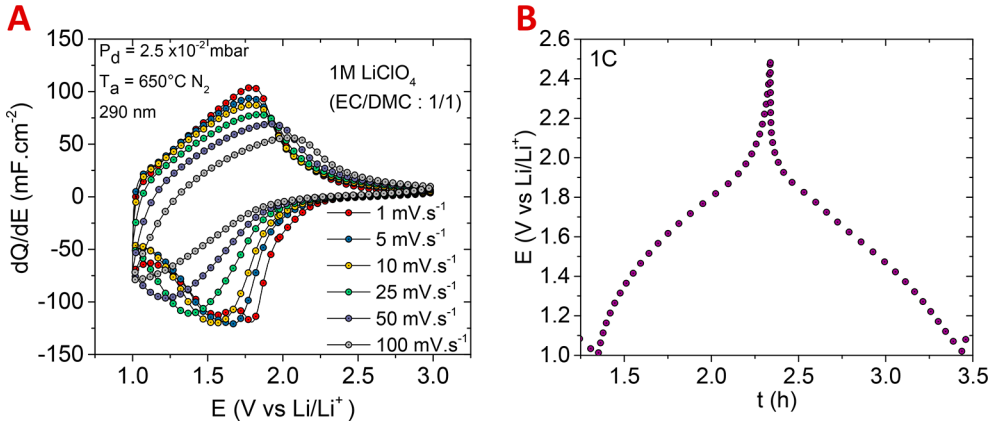

Figure 4. Electrochemistry analysis of sample S8 (thickness = 290 nm, P = 2.5 × 10^{-2} mbar, and T = 650 °C under N_2 during 5 min). The electrolyte used is 1 M $LiClO_4$ in EC/DMC (1:1). (A) Cyclic voltammetries between 1 and 3 V *vs* Li/Li$^+$ as a function of sweep rate (1 up to 100 mV·s^{-1}). (B) Galvanostatic cycling of the sample at 1C rate.

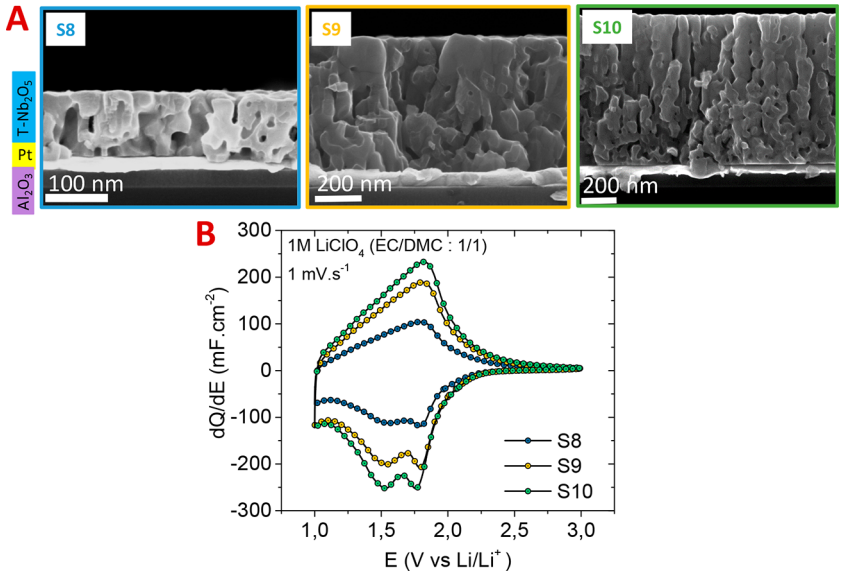

Figure 5. Study of the Nb_2O_5 performance as a function of the film thickness (P = 2.5 × 10^{-2} mbar, T = 650 °C under N_2 during 5 min). (A) SEM cross section analysis of the three Nb_2O_5 layers S9, S10, and S11. (B) Cyclic voltammetry of S8, S9, and S10 at 1 mV·s^{-1} between 1 and 3 V *vs* Li/Li$^+$.

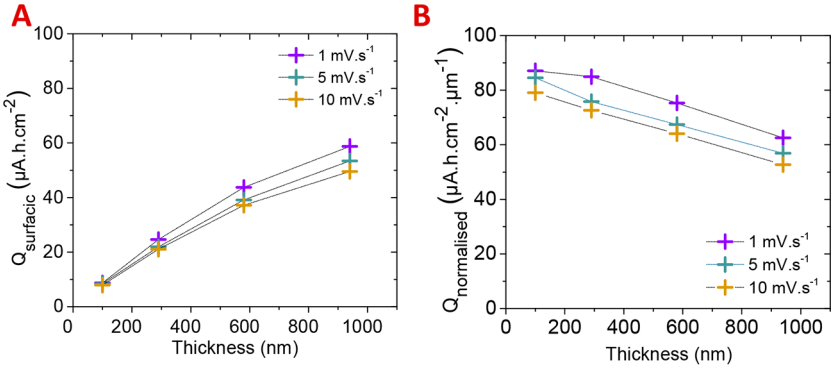

Figure 6. (A) Evolution of the surface capacity as a function of the film thickness at different sweep rates (1, 5, and 10 mV·s^{-1}) and (B) evolution of the normalized capacity delivered by the Nb_2O_5 electrodes.

observed. During the reverse scan, the set of broad anodic peaks around 1.75 and 1.5 V *vs* Li/Li$^+$ corresponding to Li-ion deintercalation from the $Li_xNb_2O_5$ host structure are also observed but a noticeable peak shift and peak separation are shown when the sweep rate increases. Moreover, the capacity remains reversible.

Constant current charge and discharge cycles of the sample are shown in Figure 4B. A capacity of 160 mAh·g^{-1} is achieved at

1C rate, with a quasi-linear change of the potential with the charge Q.

Improvement of the Electrode Performance for a Miniaturized Power Source. To fulfill the energy requirement of miniaturized IoT devices, the surface capacity of the electrode has to be improved. An attractive solution to increase the areal capacity of a mixed phase annealed at 650 °C under N_2 during 5 min and deposited at 2.5×10^{-2} mbar is to increase the thickness of the Nb_2O_5 layers. For this purpose, deposition times are varied (Table 1). From the SEM cross section imaging (Figure 5A), samples S8, S9, and S10 show a porous granular-like structure, while the charge of the CVs (Figure 5B) increases with the active mass loading (*i.e.*, the thickness) of the Nb_2O_5 electrodes. However, as shown in Figure 6A, the areal capacity measured between 3 and 1 V *vs* Li/Li^+ reaches 60 μAh·cm^{-2} at 1 mV·s^{-1} for a 0.94 μm thick Nb_2O_5 film (63.8 μAh·cm^{-2}.μm^{-1}). The surface capacity does not increase linearly with the film thickness, leading to a small decrease of the volumetric capacity (Figure 6B) for thicker layers. Nevertheless Figure SI3-A presents a plot of the cathodic and anodic peak currents observed from the voltammograms of Figure 4B as a function of sweep rate between 1 and 100 mV·s^{-1}. It is commonly accepted that in a sweep voltammetry experiment the current obeys a power-law[28] relationship with eq 2:

$$I = av^b \tag{2}$$

where I is the current (A), v is the potential sweep rate (mV·s^{-1}), and a and b are specific coefficients related to the diffusion process. The b-coefficient of sample S8 is close to 0.9 for cathodic and anodic currents, indicating that the kinetics is surface-controlled, and thus the charge storage process is fast. For S10, the b-value decreases to 0.7 and 0.75 for anodic and cathodic currents, respectively, showing the emergence of diffusion constraints or an increase of the ohmic contribution at high sweep rate (>25 mV·s^{-1}). This limitation is fundamentally different from battery materials, which are generally characterized by $b = 0.5$, indicative of a semi-infinite diffusion process.

The Nyquist plots (Figure SI3-B) of samples S8, S9, and S10 at 1.6 V *vs* Li/Li^+ exhibit an increase of the high-frequency loop and equivalent series resistance with the film thickness. This behavior can be attributed to the low electronic conductivity of the Nb_2O_5 material together with the thin film morphology that consists of large agglomerated clusters of particles with only intercolumnar porosity (spacing between columns).

CONCLUSION

The present work deals with the synthesis and electrochemical optimization of Nb_20_5 electrodes deposited by dc magnetron sputtering on an Al_2O_3/Pt-coated silicon wafer. Amorphous Nb_2O_5 thin films are sputtered on a Pt-coated silicon wafer and crystallized into a Nb_2O_5 mixed phase by annealing at 650 °C under N_2 during 5 min. The sputtering deposition pressure is tuned to promote the formation of porous niobium pentoxide films. Such synthesis conditions favor the formation of a polycrystalline structure exhibiting a porous microstructure required for efficient and fast Li-ion intercalation. The electrochemical analysis demonstrates the absence of diffusion limitations and highlights fast Li-intercalation at 1 mV·s^{-1}. Further studies dealing with the improvement of the Nb_2O_5 electronic conductivity as well as the evolution of the crystal structure upon cycling using *in situ/operando* X-ray diffraction analyses on thin film electrodes will be achieved in the near future. Such work clearly validates the important role of the electrode morphology for the fabrication of fast electrochemical energy storage devices for IoT applications.

METHODS

Thin Film Synthesis. Niobium pentoxide (Nb_2O_5) thin films are deposited by reactive direct current magnetron sputtering (dc-MS) in a CT 200 cluster from Alliance Concept using a metallic niobium target (99.9%, 10 cm diameter, 6 mm thick) under an argon and oxygen atmosphere. The distance between the target and the substrate holder is fixed to 60 mm. Depositions have been carried out on a (100) silicon substrate (diameter = 7.6 cm) coated by layers of Al_2O_3 (thickness = 100 nm) and platinum (thickness = 50 nm). The Pt layer, acting as the current collector, is evaporated using a Plassys MEB 550S apparatus, while the Al_2O_3 layer, deposited by atomic layer deposition (ALD) in a Picosun R200 reactor, acts as a diffusion barrier to prevent the Pt−Si interdiffusion responsible for the formation of a PtSi alloy, which is likely damaging the current collector.[24,25]

Before sputtering, the CT 200 cluster is pumped down to 10^{-6} mbar. The power density is kept at 1 W·cm^{-2} during the sputtering deposition, while the deposition was achieved at room temperature. Four operating pressures have been studied: 7.5×10^{-3}, 1×10^{-2}, 2.5×10^{-2}, and 5×10^{-2} mbar. The argon and oxygen flow rates are kept constant at 60 and 10 sccm, respectively. The thickness of the sputtered Nb_2O_5 layers is governed by both the deposition time and the working pressure. After synthesis, the as-deposited stacked layers (Nb_2O_5/Pt/Al_2O_3/Si) are annealed at 600, 700, or 750 °C under N_2 during 5 min in an RTA JIPELEC furnace to reach the formation of the TT-, mixed-, or T-Nb_2O_5 polymorphs, respectively. The deposition time is then increased to deposit different thickness Nb_2O_5 films.

Morphological, Structural, and Electrochemical Characterizations. The morphology and the thickness of the thin films are determined by SEM) with a Zeiss Ultra electron microscope. The surface roughness is measured by atomic force microscopy (AFM Dimension 3100). To investigate the structure and the crystalline orientation of obtained films, a Rigaku Smartlab multipurpose 6-axis diffractometer (9 kW rotating anode) is used in a high-resolution parallel beam mode (with Soller slits of 5° and a PSD 1D detector DTEX) delivering Cu Kα radiation (lambda = 1.5406 Å). *In situ* X-ray diffraction measurements are performed in a temperature range from 25 to 1000 °C using a DHS 1100 air-filled chamber.

Electrochemical characterizations of the thin films were conducted in cells operated in an Ar-filled Fibox. The cells are assembled in a glovebox under an Ar atmosphere, using a Nb_2O_5 thin film as working electrode and pure lithium metal (Sigma-Aldrich) as both reference and counter electrodes. A mixture of 1 M lithium perchlorate salt ($LiClO_4$ Sigma-Aldrich) dissolved in EC and DMC, in 1:1 proportion, is used as the liquid electrolyte. Cyclic voltammetry, electrochemical impedance spectroscopy (EIS), and galvanostatic cycling with potential limitations were performed using a multichannel Biologic VMP3 potentiostat in a two-electrode configuration. EIS measurements are conducted after cycling by applying a 5.0 mV_{RMS} sinusoidal signal amplitude from 100 kHz to 10 mHz at the open-circuit potential at different voltages (from 2 down to 1.1 V *vs* Li/Li^+).

ASSOCIATED CONTENT

Supporting Information

The Supporting Information is available free of charge on the ACS Publications website at DOI: 10.1021/acsnano.9b01457.

> Structural, morphological, and electrochemical analyses of T-Nb_2O_5 annealed under an air atmosphere; diffractograms of the Nb_2O_5 films deposited at different pressures; kinetic analysis of the films exhibiting various thicknesses; electrochemical impedance spectroscopy analysis of the film deposited with the optimized pressure and annealed at suitable temperature (PDF)

AUTHOR INFORMATION

Corresponding Authors

*E-mail: simon@chimie.ups-tlse.fr.
*E-mail: Christophe.lethien@univ-lille.fr.

ORCID

Pascal Roussel: 0000-0001-7243-7293
Patrice Simon: 0000-0002-0461-8268
Christophe Lethien: 0000-0001-8906-8308

Notes

The authors declare no competing financial interest.

ACKNOWLEDGMENTS

This research is financially supported by the ANR within the MINOTORES project. The French Renatech network is greatly acknowledged for the microfabrication facilities. The authors also want to thank the French network on electrochemical energy storage (RS2E) and the STORE-EX ANR project for the support. The Ministère de l'Enseignement Supérieur et de la Recherche, Région Hauts de France and FEDER are acknowledged for supporting and funding XRD facilities.

REFERENCES

(1) Lethien, C.; Le Bideau, J.; Brousse, T. Challenges and Prospects of 3D Micro-Supercapacitors for Powering the Internet of Things. *Energy Environ. Sci.* **2019**, *12*, 96−115.

(2) Huang, P.; Lethien, C.; Pinaud, S.; Brousse, K.; Laloo, R.; Turq, V.; Respaud, M.; Demortiere, A.; Daffos, B.; Taberna, P. L.; Gogotsi, Y.; Simon, P. On-Chip and Freestanding Elastic Carbon Films for Micro-Supercapacitors. *Science* **2016**, *351* (6274), 691−695.

(3) Pech, D.; Brunet, M.; Durou, H.; Huang, P.; Mochalin, V.; Gogotsi, Y.; Taberna, P.-L.; Simon, P. Ultrahigh-Power Micrometre-Sized Supercapacitors Based on Onion-like Carbon. *Nat. Nanotechnol.* **2010**, *5*, 651−654.

(4) González, A.; Goikolea, E.; Barrena, J. A.; Mysyk, R. Review on Supercapacitors: Technologies and Materials. *Renewable Sustainable Energy Rev.* **2016**, *58* (C), 1189−1206.

(5) Iwama, E.; Kisu, K.; Naoi, W.; Simon, P.; Naoi, K. Enhanced Hybrid Supercapacitors Utilizing Nanostructured Metal Oxides. In *Metal Oxides in Supercapacitors*; Elsevier Inc., 2017; pp 247−264.

(6) Kim, H. S.; Cook, J. B.; Lin, H.; Ko, J. S.; Tolbert, S. H.; Ozolins, V.; Dunn, B. Oxygen Vacancies Enhance Pseudocapacitive Charge Storage Properties of MoO3-X. *Nat. Mater.* **2017**, *16*, 454−462.

(7) Brezesinski, T.; Wang, J.; Tolbert, S. H.; Dunn, B. Ordered Mesoporous α-MoO3 with Iso-Oriented Nanocrystalline Walls for Thin-Film Pseudocapacitors. *Nat. Mater.* **2010**, *9*, 146.

(8) Fehse, M.; Ventosa, E. Is TiO2(B) the Future of Titanium-Based Battery Materials? *ChemPlusChem* **2015**, *80*, 785−795.

(9) Zukalová, M.; Kalbáč, M.; Kavan, L.; Exnar, I.; Graetzel, M. Pseudocapacitive Lithium Storage in TiO2(B). *Chem. Mater.* **2005**, *17*, 1248−1255.

(10) Wang, J.; Polleux, J.; Lim, J.; Dunn, B. Pseudocapacitive Contributions to Electrochemical Energy Storage in TiO 2 (Anatase) Nanoparticles. *J. Phys. Chem. C* **2007**, *111*, 14925−14931.

(11) Wang, J.; Polleux, J.; Brezesinski, T.; Tolbert, S.; Dunn, B. The Pseudocapacitive Behavior of TiO 2 (Anatase) Nanoparticles. *ECS Trans* **2007**, *11*, 101−111.

(12) Brezesinski, T.; Wang, J.; Polleux, J.; Dunn, B.; Tolbert, S. H. Templated Nanocrystal-Based Porous TiO2 Films for Next-Generation Electrochemical Capacitors. *J. Am. Chem. Soc.* **2009**, *131*, 1802−1809.

(13) Kim, H.-S.; Cook, J. B.; Tolbert, S. H.; Dunn, B. The Development of Pseudocapacitive Properties in Nanosized-MoO 2. *J. Electrochem. Soc.* **2015**, *162*, A5083−A5090.

(14) Lesel, B. K.; Ko, J. S.; Dunn, B.; Tolbert, S. H. Mesoporous LixMn2O4 Thin Film Cathodes for Lithium-Ion Pseudocapacitors. *ACS Nano* **2016**, *10*, 7572−7581.

(15) Kumagai, N. Thermodynamics and Kinetics of Lithium Intercalation into Nb2O5 Electrodes for a 2 V Rechargeable Lithium Battery. *J. Electrochem. Soc.* **2002**, *146*, 3203.

(16) Kim, J. W.; Augustyn, V.; Dunn, B. The Effect of Crystallinity on the Rapid Pseudocapacitive Response of Nb2O5. *Adv. Energy Mater.* **2012**, *2*, 141−148.

(17) Come, J.; Augustyn, V.; Kim, J. W.; Rozier, P.; Taberna, P.-L.; Gogotsi, P.; Long, J. W.; Dunn, B.; Simon, P. Electrochemical Kinetics of Nanostructured Nb2O5 Electrodes. *J. Electrochem. Soc.* **2014**, *161*, A718−A725.

(18) Ohzuku, T.; Sawai, K.; Hirai, T. Electrochemistry of L-Niobium Pentoxide a Lithium/Non-Aqueous Cell. *J. Power Sources* **1987**, *19*, 287−299.

(19) Lai, C.-H.; Ashby, D.; Moz, M.; Gogotsi, Y.; Pilon, L.; Dunn, B. Designing Pseudocapacitance for Nb_2O_5/Carbide-Derived Carbon Electrodes and Hybrid Devices. *Langmuir* **2017**, *33*, 9407−9415.

(20) Schultze, J. W.; Lohrengel, M. M. Stability, Reactivity and Breakdown of Passive Fi Lms.Problems of Recent and Future Research. *Electrochim. Acta* **2000**, *45*, 2499−2513.

(21) Kats, E.; Zhuiykov, S. Development of Quasi-Two-Dimensional Nb2O5 for Functional Electrodes of Advanced Electrochemical Systems. *Int. J. Chem., Mol., Nucl., Mater. Metallurgical Eng.* **2013**, 353−359.

(22) Augustyn, V.; Come, J.; Lowe, M. A.; Kim, J. W.; Taberna, P.-L.; Tolbert, S. H.; Abruña, H. D.; Simon, P.; Dunn, B. High-Rate Electrochemical Energy Storage through Li+ Intercalation Pseudocapacitance. *Nat. Mater.* **2013**, *12*, 518−522.

(23) Ouendi, S.; Arico, C.; Blanchard, F.; Codron, J.-L.; Wallart, X.; Taberna, P. L.; Roussel, P.; Clavier, L.; Simon, P.; Lethien, C. Synthesis of T-Nb2O5 Thin-Films Deposited by Atomic Layer Deposition for Miniaturized Electrochemical Energy Storage Devices. *Energy Storage Mater.* **2019**, *16*, 581−588.

(24) Hallot, M.; Lethien, C.; Brousse, T.; Létiche, M.; Roussel, P.; Huvé, M. Tuning the Cation Ordering with the Deposition Pressure in Sputtered LiMn 1.5 Ni 0.5 O 4 Thin Film Deposited on Functional Current Collectors for Li-Ion Microbattery Applications. *Chem. Mater.* **2017**, *29*, 6044−6057.

(25) Hallot, M.; Demortière, A.; Roussel, P.; Lethien, C. Sputtered LiMn1.5Ni0.5O4 Thin Films for Li-Ion Micro-Batteries with High Energy and Rate Capabilities. *Energy Storage Mater.* **2018**, *15*, 396−406.

(26) Robert, K.; Douard, C.; Demortière, A.; Blanchard, F.; Roussel, P.; Brousse, T.; Lethien, C. On Chip Interdigitated Micro-Supercapacitors Based on Sputtered Bifunctional Vanadium Nitride Thin Films with Finely Tuned Inter- and Intracolumnar Porosities. *Adv. Mater. Technol.* **2018**, *3*, 1800036.

(27) Kumagai, N.; Tateshita, Y.; Takatsuka, Y.; Baba, M.; Ikeda, T.; Tanno, K. Intercalation of Lithium in r.f.-Sputtered Niobium Oxide Film as Electrode Material for Lithium-Ion Batteries. *J. Power Sources* **1995**, *54*, 175−179.

(28) Lindström, H.; Södergren, S.; Solbrand, A.; Rensmo, H.; Hjelm, J.; Hagfeldt, A.; Lindquist, S.-E. Li+ Ion Insertion in TiO2 (Anatase). 2. Voltammetry on Nanoporous Films. *J. Phys. Chem. B* **1997**, *101*, 7717−7722.

Fast Electrochemical Storage Process In Sputtered Nb_2O_5 Porous Thin Films

Supporting Information

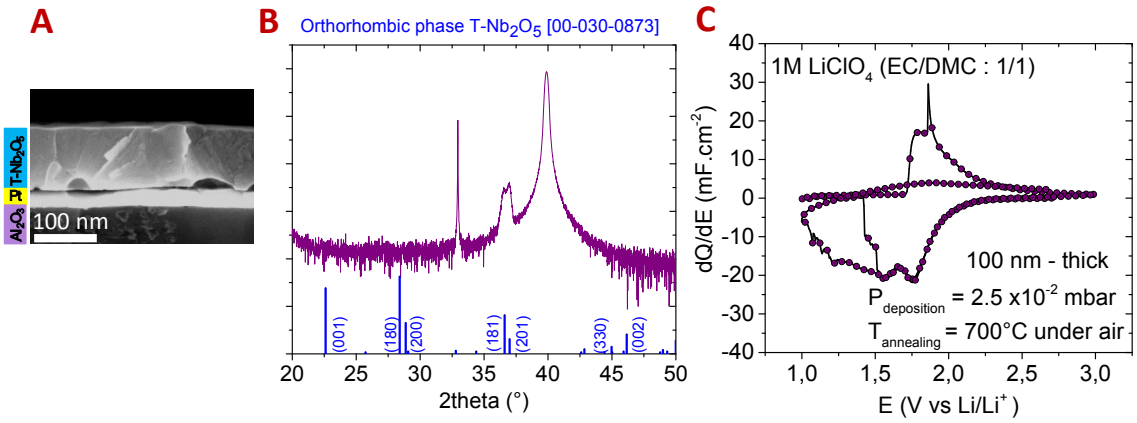

Figure SI1: A. SEM cross section analysis of the Nb_2O_5 thin film deposited at 2.5 x10^{-2} mbar and annealed under air at 700°C during 2h. **B.** X-ray diffraction analysis after air annealing showing a preferential orientation at 36.7°. **C.** First two cycles of cyclic

voltammetry at 1 mV.s^{-1} showing the current leakage, consequently the thin film delamination.

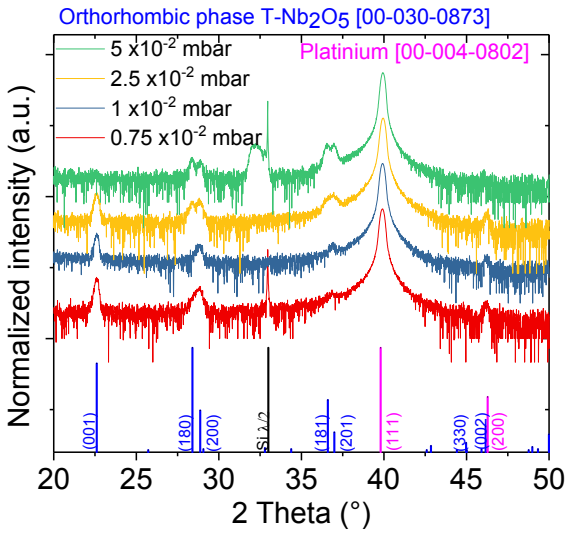

Figure SI2: Diffractogramms of the S1-S4 samples as a function of the deposition pressures (700 °C).

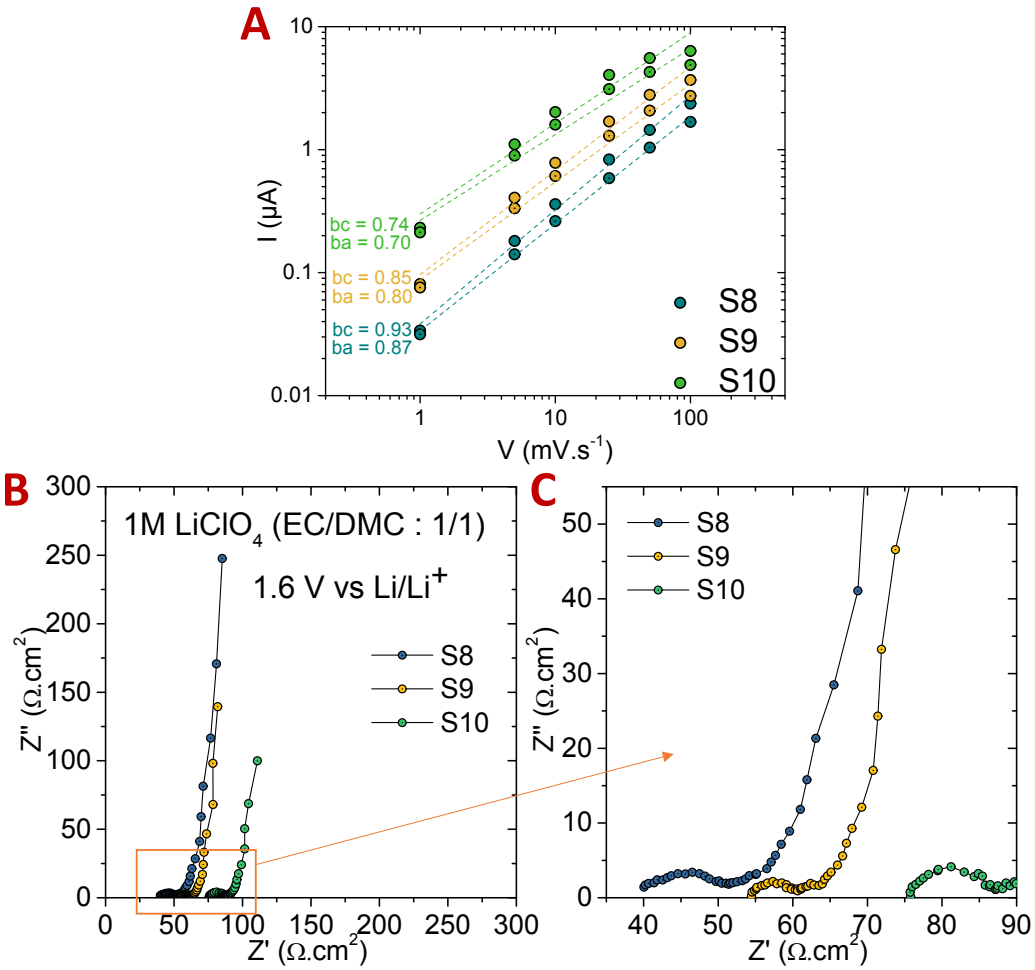

Figure SI3: Nb_2O_5 thin films deposited with different thicknesses annealed at 650 °C under N_2 during 5 minutes. **A.** Cathodic and anodic currents as a function of sweep rate. **B**. Nyquist plots spectra between 100 KHz and 10 mHz at 1.6 V vs Li/Li^+. **C.** Focus on the high frequency.

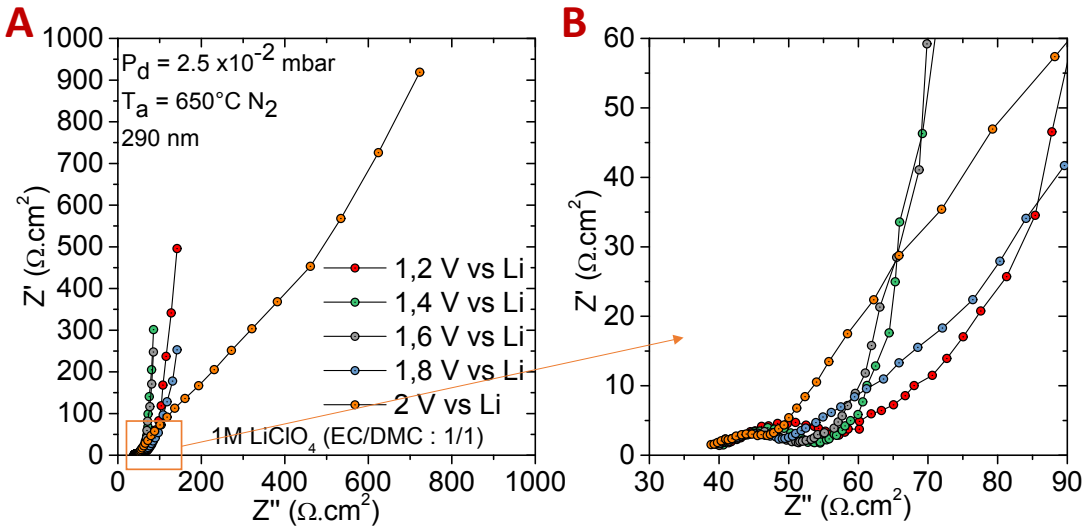

Figure SI4: A. Nyquist plots spectra between 100 KHz and 10 mHz as a function of the applied potential vs Li/Li^+. **B.** Focus on the high frequency.

Electrochemical impedance spectroscopy (EIS) study is achieved to get a better understanding of the lithium ion transport process into the Nb_2O_5 electrode. EIS measurements are made at constant potentials between 2.0 and 1.2 V vs Li/Li^+, i.e. in the redox active region of the crystallized Nb_2O_5 electrode. Nyquist plots presented in **figure SI4A and SI4B** show a small loop in the high frequency region (about 10 ohm.cm²) which does not change with the bias potential applied. Such a high frequency loop is connected to the contact impedance at the substrate / Nb_2O_5 film interface. The high frequency resistance (Equivalent Serie Resistance ESR) are measured at 40 ohm.cm², which stays

low, thanks to the small thickness of the Nb_2O_5 film. When the frequency is decreased, the Nyquist plot shows the typical features of a pseudocapacitive charge storage mechanism with a fast, quasi-vertical increase of the imaginary part of the impedance, resulting from the fast, pseudocapacitive Li intercalation reaction mechanism in the Nb_2O_5., as previously reported[27]